

Simulating the Formation of Primordial Proto-Stars

Naoki Yoshida

Department of Physics, Nagoya University, Furocho, Chikusa, Nagoya 464-8602, Japan

Abstract. We study the formation of primordial proto-stars in a Λ CDM universe using high-resolution cosmological simulations. Our approach includes all the relevant atomic and molecular physics necessary to follow the thermal evolution of a prestellar gas cloud to very high densities. We describe the numerical implementation of the physics. We show the results of a simulation of the formation of primordial stars in a reionized gas.

Keywords: Population III Stars

PACS: 97.20.Wt

PHYSICS OF PRIMORDIAL STAR FORMATION

The study of primordial star formation has a long history. The formation of the first cosmological objects via gas condensation by molecular hydrogen cooling has been studied for many years since late 1960's. One-dimensional hydrodynamic simulations of spherical gas collapse were performed by a number of researchers. Omukai & Nishi [1] included a detailed treatment of all the relevant chemistry and radiative processes and thus were able to provide accurate results on the thermal evolution of a collapsing primordial gas cloud up to stellar densities. These authors found that, while the evolution of a spherical primordial gas cloud proceeds in a roughly self-similar manner, there are a number of differences in the thermal evolution from that of present-day, metal- and dust-enriched gas clouds.

Recently, three-dimensional hydrodynamic calculations were performed by several groups. Statistical properties of primordial star-forming clouds and the overall effect of cosmological bias have been studied in detail [2, 3]. Simulations of the formation of primordial proto-stars have been hampered by the complexity of the involved physics, such as radiative transfer in very high-density primordial gases. A critical technique we describe in this contribution is computation of molecular line opacities and continuum opacities. With the implementation of optically thick cooling, the gas evolution can be accurately followed to much higher densities than was possible in the previous studies [4, 6]. We show that the method works well in problems of collapsing gas clouds, in terms of computation of radiative cooling rates and resulting density and temperature structure. Our method can be applied to a broad range of three-dimensional problems in non-trivial configurations. We apply this technique to a cosmological simulation of the formation of primordial star.

OPTICALLY THICK COOLING RATE

Molecular hydrogen line cooling

When the gas density and the molecular fraction are high, the cloud becomes opaque to molecular lines and then H_2 line cooling becomes inefficient. The net cooling rate can be expressed as

$$\Lambda_{H_2, \text{thick}} = \sum_{u,l} h\nu_{ul} \beta_{\text{esc},ul} A_{ul} n_u, \quad (1)$$

where n_u is the population density of hydrogen molecules in the upper energy level u , A_{ul} is the Einstein coefficient for spontaneous transition, $\beta_{\text{esc},ul}$ is the probability for an emitted line photon to escape without absorption, and $h\nu_{ul} = \Delta E_{ul}$ is the energy difference between the two levels.

In order to calculate the escape probability, we first evaluate the opacity for each molecular line as

$$\tau_{lu} = \alpha_{lu} L, \quad (2)$$

where L is the characteristic length scale. Since the absorption coefficients α_{lu} are computed in a straightforward manner, although somewhat costly, the remaining key task is the evaluation of the length scale L . By noting that the important quantity we need is the effective gas cooling rate, we can formulate a reasonable and well-motivated approximation. To this end, we decided to use the Sobolev method that is widely used in the study of stellar winds and planetary nebulae.

We calculate the Sobolev length along a line-of-sight as

$$L_r = \frac{v_{\text{thermal}}}{|dV_r/dr|}, \quad (3)$$

where $v_{\text{thermal}} = \sqrt{kT/m_H}$ is the thermal velocity of H_2 molecules, and V_r is the fluid velocity in the direction. A suitable angle-average must be computed in order to obtain the net escape probability. Details are found in [4].

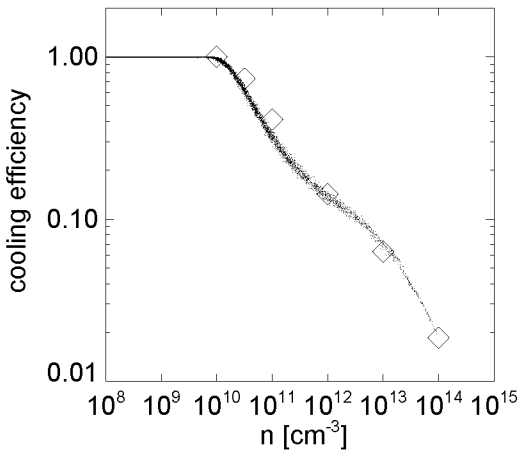


FIGURE 1. The effect of molecular line opacities to the net cooling rate.

We test our method by performing a three-dimensional calculation of spherical cloud collapse. Figure 1 shows the normalized H_2 line cooling rate against local density. We use an output at the time when the central density is $n_c = 10^{14} \text{cm}^{-3}$. In the figure, we compare our simulation results with those from the full radiative transfer calculations of [1] (open diamonds). Clearly, our method works very well. The steepening of the slope at $n > 10^{12} \text{cm}^{-3}$, owing to the velocity change where infalling gas settles gradually onto the center, is well-reproduced. We emphasize that the level of agreement shown in Figure 1 can be achieved only if *all* of the local densities (of chemical species), temperatures, and velocities are reproduced correctly.

Cooling by collision-induced emission

Next, we implement computation of local optical depth to continuum radiation using the Planck opacity table of Lenzuni et al. [7]. The continuum opacity is used to evaluate the net cooling rate by collision-induced emission (CIE). The optically thin cooling rate can be computed as in [4].

Figure 2 compares the opacities for a gas of primordial composition calculated by Lenzuni et al. [7] and Mayer & Duschl [8]. We find no significant difference between the two opacity tables, and thus we use the one by Lenzuni et al. We calculate local optical depths in six orthogonal directions from a target point in a smoothed particle hydrodynamics manner (see, e.g., [5]), by projecting the SPH kernels of surrounding gas particles which have their own density and temperature. The net energy trans-

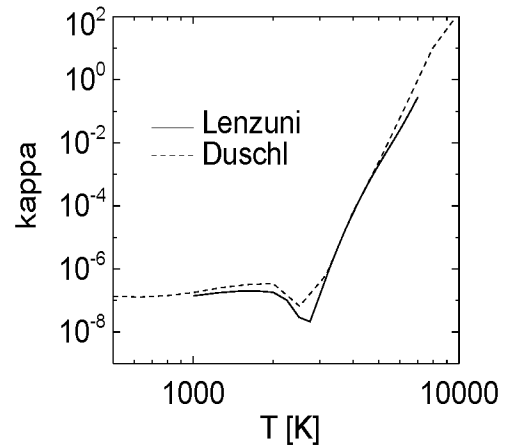


FIGURE 2. The Planck opacity as a function of temperature for a density of 10^{16}cm^{-3} .

fer rate in each direction scales as $\propto 1/(1 + \tau)$ when the optical depth is small. Again, a suitable angle average must be calculated. We simply take the mean of six directions,

$$f_{\text{reduce}} = \frac{1}{6} \sum \frac{1}{1 + \tau_i}. \quad (4)$$

We then use this local reduction factor to evaluate the cooling rate¹ Figure 3 shows the net reduction factor for the CIE cooling rate against local density. We note that, although our method is still approximate, it takes into account local density, temperature, and their structures (geometry) in a self-consistent manner. Our method can be applied to general problems, whereas simple functional fits that is based only on local density will fail in estimating the true cooling rate when the cloud core has a complex structure such as (weak) turbulence.

DISSOCIATION COOLING

When a gas cloud core becomes opaque to continuum radiation, the gas can still absorb thermal energy input owing to gravitational contraction by dissociating molecules. Ionization cooling is unimportant in the temperature regime we consider.

For densities much larger than 10^{15}cm^{-3} , the reaction time scale becomes significantly shorter than the dynamical time. Then, we can use equilibrium chemistry, which would actually *simplify* our handling of chemistry evolu-

¹ This estimate becomes incorrect when τ is large. However, the radiative cooling rate is extremely small for large τ and so the exact behavior at very optically-thick regime does not matter to the net cooling rate.

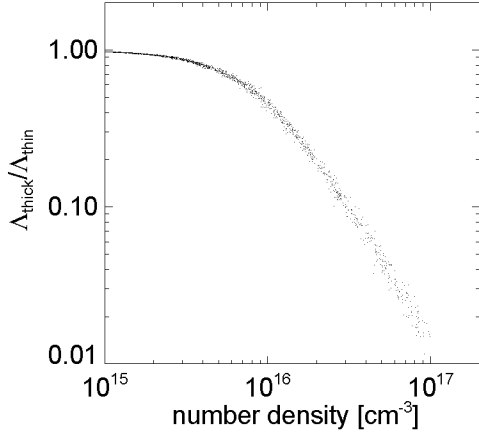


FIGURE 3. The ratio of $\Lambda_{\text{CIE,thick}}/\Lambda_{\text{CIE,thin}}$ as a function of density. We use an output when the central density reaches 10^{20}cm^{-3} .

tion. The species abundances can be determined from the coupled Saha-Boltzmann equations:

$$\frac{n(\text{H})^2}{n(\text{H}_2)} = \frac{z_{\text{H}}^2}{z_{\text{H}_2}} \left(\frac{\pi k m_{\text{H}}}{h^2} \right)^{3/2} T^{3/2} \exp\left(-\frac{\chi_{\text{H}_2}}{kT}\right), \quad (5)$$

$$\frac{n(\text{H}^+)^2}{n(\text{H})} = \frac{2}{z_{\text{H}}} \left(\frac{2\pi k m_{\text{e}}}{h^2} \right)^{3/2} T^{3/2} \exp\left(-\frac{\chi_{\text{H}}}{kT}\right). \quad (6)$$

We solve these equations at a given gas density iteratively. The associated cooling/heating due to dissociation/formation is implemented self-consistently as

$$\epsilon_{\text{H}_2} = \chi_{\text{H}_2} \Delta n_{\text{H}_2} \quad (7)$$

where $\chi_{\text{H}_2} = 4.48 \text{eV}$ is the molecular binding energy.

When dissociation of hydrogen molecules is completed at $T \sim 5000 \text{K}$, there will be no further mechanisms that enable the gas to lose its thermal energy, and then the gas temperature increases following the so-called adiabatic track.

The equation of state in the high pressure regime must be modified to account for various non-ideal gas effects [9]. Figure 4 shows the effective gas pressure for which various non-ideal gas effects are included.

PRIMORDIAL STAR FORMATION IN A REIONIZED GAS

We employ the technique described in the previous sections in a cosmological simulation. Earlier [5], we used a large cosmological simulation to study the evolution of early relic HII regions until second-generation gas clouds

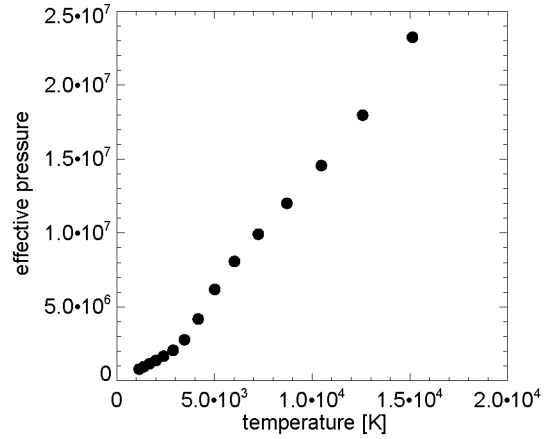


FIGURE 4. Pressure for a non-ideal gas, as calculated by [9], for a particle number density of 10^{19}cm^{-3} .

are formed. We further explore the evolution of these prestellar gas clouds. The highest density achieved by the simulation is $\sim 10^{18} \text{cm}^{-3}$, at which point the central core is optically thick even to continuum radiation. Full-scale dissociation of hydrogen molecules is taking place in the core, which works as an effective *cooling* mechanism. We investigate in detail the structure of such gas clouds. We then compute the gas mass accretion rate and use it as an input to a proto-stellar calculation.

Figure 5 shows the radial temperature profile around the proto-star and the gas mass accretion rate. The temperature structure can be understood by appealing to various atomic and molecular processes (see [4, 6]). HD line cooling brings the gas temperature below 100 Kelvin. Note that the minimum temperature is set by the cosmic microwave background.

The central proto-stellar ‘seed’ is accreting the surrounding gas at a rate $> 10^{-3} M_{\odot}/\text{yr}$, and thus a star with mass $\sim 10 M_{\odot}$ will form within 10^4 years. However, the final stellar mass is determined by processes such as radiative feedback from the protostar. We treat the evolution of a protostar as a sequence of a growing hydrostatic core with an accreting envelope. The ordinary stellar structure equations are applied to the hydrostatic core. The structure of the accreting envelope is calculated under the assumption that the flow is steady for a given mass accretion rate.

Figure 6 shows the resulting evolution of the protostar. After a transient phase and an adiabatic growth phase at $M_* < 10 M_{\odot}$, the protostar enters the Kelvin-Helmholtz phase and contracts by radiating its thermal energy. When the central temperature reaches 10^8K , hydrogen burning by the CNO cycle begins with a slight amount of carbon synthesized by helium burning. This phase is marked by a solid circle in the figure. The en-

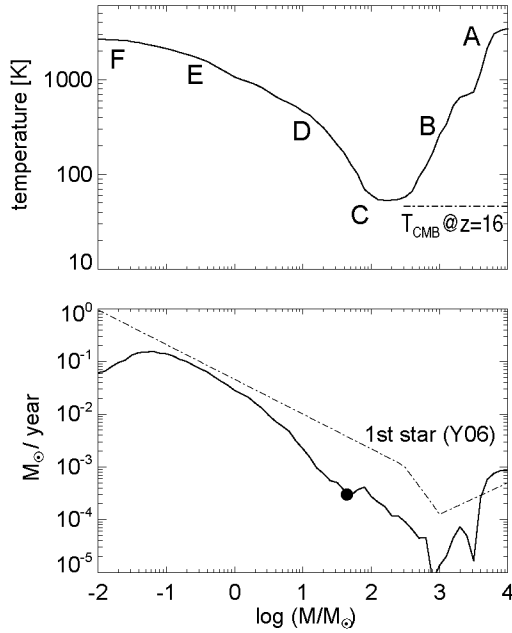


FIGURE 5. (Top) The radial temperature profile around the proto-star as a function of enclosed gas mass. (Bottom) The instantaneous gas mass accretion rate. We also show the accretion rate of [4].

ergy generation by hydrogen burning halts contraction when the mass is $35M_{\odot}$ and its radius is ~ 2.8 solar radii. Soon after, the star reaches the zero-age main sequence (ZAMS). The protostar relaxes to a ZAMS star within about 10^5 years from the birth of the protostellar seed. Accretion is not halted by radiation from the protostar to the end of our calculation.

It is important to point out that the mass of the parent cloud from which the star formed is $M_{\text{cloud}} \sim 40M_{\odot}$. The final stellar mass is likely limited by the mass of the gravitationally unstable parent cloud. We thus argue that primordial stars formed from an ionized gas are massive, with a characteristic mass of several tens of solar masses, allowing overall uncertainties in the accretion physics and also the dependence of the minimum gas temperature on redshift. They are smaller than the first stars formed from a neutral gas, but are not low-mass objects as suggested by earlier studies.

The elemental abundance patterns of recently discovered hyper metal-poor stars suggest that they might have been born from the interstellar medium that was metal-enriched by supernovae of these massive primordial stars.

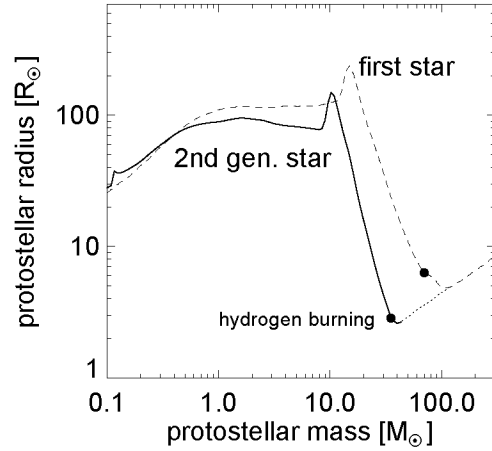


FIGURE 6. Evolution of the proto-stellar radius and the mass (solid line). The solid circle marks the time when efficient hydrogen burning begins. The dotted line shows the mass (and radius) growth which is calculated under the assumption that a larger amount of gas than the parent cloud can be accreted. For reference we also show the result from Y06 for a first generation star that forms in an initially neutral gas cloud.

ACKNOWLEDGMENTS

The work is supported in part by the Grants-in-Aid for Young Scientists 17684008 by the Ministry of Education, Culture, Science and Technology of Japan, and by The Mitsubishi Foundation.

REFERENCES

1. Omukai, K. & Nishi, R., 1998, *ApJ*, 508, 141
2. Yoshida, N., Abel, T., Hernquist, L., Sugiyama, N., 2003, *ApJ*, 592, 645
3. Gao, L., Yoshida, N., Abel, T., Frenk, C. S., Jenkins, A., Springel, V., 2007, *MNRAS*, 378, 449
4. Yoshida, N., Omukai, K., Hernquist, L., Abel, T., 2006, *ApJ*, 652, 6
5. Yoshida, N., Oh, S.-P., Kitayama, T., Hernquist, L., 2007, *ApJ*, 663, 687
6. Yoshida, N., Omukai, K., Hernquist, L., 2007, *ApJL*, 667 (October 1 issue)
7. Lenzuni, P., D., Chernoff, D. F., & Salpeter, E. E., 1991, *ApJS*, 76, 759
8. Mayer, M. & Duschl, W.J., 2005, *MNRAS*, 358, 614
9. Saumon, D., Chabrier, G., & van Horn, H. M., 1995, *ApJS*, 99, 713

Copyright of AIP Conference Proceedings is the property of American Institute of Physics and its content may not be copied or emailed to multiple sites or posted to a listserv without the copyright holder's express written permission. However, users may print, download, or email articles for individual use.